Hindawi
Geofluids
Volume 2018, Article ID 8127207, 11 pages
https://doi.org/10.1155/2018/8127207

WILEY | Hindawi

Research Article

A Gas Seepage Modeling Study for Mitigating Gas Accumulation Risk in Upper Protective Coal Seam Mining Process

Cun Zhang,[1,2] **Lei Zhang**,[3] **Mingxue Li**,[4] **and Chen Wang**[2,5]

[1]*Beijing Key Laboratory for Precise Mining of Intergrown Energy and Resources, China University of Mining & Technology (Beijing), Beijing 100083, China*
[2]*State Key Laboratory of Coal Resources and Safe Mining (CUMT), Xuzhou, Jiangsu 221116, China*
[3]*Key Laboratory of Deep Coal Resource Ministry of Education of China, School of Mines, China University of Mining & Technology, Xuzhou, Jiangsu 221116, China*
[4]*School of Physics, China University of Mining & Technology, Xuzhou, Jiangsu 221116, China*
[5]*Mining College, Guizhou University, Guiyang 550025, China*

Correspondence should be addressed to Cun Zhang; cumt_zc@163.com and Chen Wang; cwang@gzu.edu.cn

Received 10 May 2018; Accepted 6 September 2018; Published 23 December 2018

Guest Editor: Wen Wang

Protective coal seam mining (PCSM) is one of the most significant mitigation measures of regional outburst in the process of deep coal seam mining, which has high outburst risk in China. During the PCSM process, the phenomenon of methane concentration exceeding the limit usually occurs in the working face. It is vital to understand factors affecting gas emission from the protective seam working face (PSWF) and to obtain an equation for determining the quantity of gas emission. A gas seepage model (GSM) was developed to simulate the gas emission during the process of upper PCSM. In this study, an equation was formulated to determine the quantity of gas desorbed from the protected seam into PSWF. These equations have been developed by using Fick's second law of diffusion and Darcy's flow law. The relationship between permeability and stress was described in an elastic-plastic state, and the mechanics of surrounding rock were investigated. It can be concluded from GSM that the initial gas pressure of protected seam, the characteristics of interlayer rocks, and the ventilation pressure of PSWF were the main factors that influenced the desorption of gas emission from the protected seam into PSWF. The developed GSM was tested for calculating gas emission quantity from the PCSM process by utilizing the actual geological condition data of a coal mine, which is located in Hancheng, China. The results have shown great agreement with obtained field measurements, which is done by combining the fitting curve of ventilation air methane quantity for PSWF with an interlayer spacing. A loss coefficient (δ) of 1.012×10^{-3} was obtained in this study.

1. Introduction

Coal and gas outburst accident is a complex dynamic phenomenon, which occurs frequently in coal mines in China. Because of its sudden occurrence and intense destructiveness, the accident endangers both coal mine production and personnel safety. It also causes immense economic losses to mining companies [1–3]. To address this issue, many research studies have been conducted nationally. These studies have elucidated the outburst mechanism in coal and gas; moreover, outburst risk indexes and mitigation measures have been proposed in these studies [4–6]. Protective coal seam mining (PCSM) is preferentially used to release coal seam pressure and enhance permeability. It is one of the main outburst mitigation measures in China, mainly because gas content and its associated outburst risk are relatively low. By extracting the protective seam, the associated pressure is released and it substantially increases the permeability of the protected seam. Pressure relief gas extraction is enhanced consequently [7–9]. During protective coal seam mining (PCSM), the phenomenon of methane concentration exceeding the limit usually occurs in the protective seam working face (PSWF). Because the protected seam offers gas pressure relief, a large amount of gas is desorbed and flows into PSWF.

This is the main reason why methane concentration exceeds the limit in the PCSM process. To guarantee safe mining and to improve methane mining, pressure relief gas extraction technology is used currently [10–12]. Presently, more attention is paid to pressure relief effect of the protected seam, but factors causing methane concentration to exceed the limit are ignored during PCSM [13, 14]. A qualitative method is mainly used to estimate pressure relief gas seepage, which is not applicable for gas drainage and control [15–17]. Besides, there are few studies on the main influencing factors of pressure relief gas seepage. It is also not conducive to the extraction and control of pressure relief gas. Thus, a quantitative analysis of seepage characteristics of pressure relief gas is of great significance to the layout of gas drainage boreholes and the mining parameters of protective coal seam.

In this paper, previous studies on coal and rock permeability have been summarized. Stress-strain relationship, stress changes, and failure depth of the floor have been determined in the process of PCSM. Based on review results, GSM is established and its equation is used for calculating the quantity of gas desorbed from the protected seam into the protective seam during PCSM. The influencing factors were also identified by analyzing the seepage process. Finally, the model is validated with the data from an in situ ventilation air methane of the PSWF in a coal mine, which is located in Hancheng, China. The results indicate that the established GSM completely agreed with obtained field measurements.

2. Previous Studies on the Evolution Law of Permeability

Ever since the proposition of Darcy's law, rock permeability research has always been an attractive and ongoing research field. After years of development and research, two main types of the permeability model were established: porosity-permeability model and stress-permeability model. These models are represented by Palmer-Mansoori's (P-M) and Gray's model, respectively [18]. In the coal permeability model proposed by Gray [19], ground and expansion/shrinkage stress caused by adsorption/desorption gases was investigated comprehensively.

$$\sigma_h^e - \sigma_{h0}^e = -\frac{\nu}{1-\nu}(p - p_0) + \frac{E}{1-\nu}\frac{\Delta\varepsilon_s}{\Delta p_s}\Delta p_s. \tag{1}$$

Here, σ_h^e is the effective horizontal stress, which is expressed in MPa; σ_{h0}^e is the initial effective horizontal stress, which is expressed in MPa; Δp_s is the change in adsorption equilibrium pressure, which is expressed in MPa; $\Delta\varepsilon_s$ is the strain change in unit, which is caused by change in adsorption equilibrium pressure; ν is the Poisson's ratio; p is gas pressure and p_0 is initial gas pressure, which are expressed in MPa; and E is the elastic modulus in GPa.

As shown in (2), Seidle et al. [20] proposed a more concise expression.

$$k = k_0 e^{-3c_f(\sigma-\sigma_0)}. \tag{2}$$

Herein, c_f is the cleat volume compressibility with respect to changes in effective stress normal to the cleat, k_0 is initial cleat permeability at initial effective stress σ_0, and k is cleat permeability at effective stress σ.

Equation (2) has been used in several laboratory experiments, which have been conducted to develop fitting regression equations. As shown in (3), Ren and Edwards [21] proposed that permeability and stress relation were associated with intact rock.

$$k = k_0 e^{-0.25(\sigma-\sigma_0)}. \tag{3}$$

Whittles et al. [22] summarized the relationship between the permeability of rock fracture surface and principal stress. Equation (4) is used for calculating fracture surface permeability.

$$k = k_1\left(\frac{\sigma_1+\sigma_3}{2}\right)^m. \tag{4}$$

Here, σ_1 and σ_3 are minimum and maximum confining stresses, respectively, which are expressed in MPa; k_1 is intrinsic permeability expressed in m^2 when $(\sigma_1+\sigma_3)/2 = 1$ MPa; and m is a material parameter found by regression analysis. In a study conducted by Whittles et al., the values of -0.8616 and 2.613×10^{-13} m^2 were determined for m and k_1, respectively. [22].

The most representative permeability model proposed by Palmer and Mansoori [23] and Palmer et al. [24] was expressed as

$$\left.\begin{aligned}
&\frac{\varphi}{\varphi_0} = 1 + \frac{c_m}{\varphi_0}(p-p_0) + \frac{\varepsilon_1}{\varphi_0}\left(\frac{K}{M}-1\right)\left(\frac{p}{p_\varepsilon+p} - \frac{p_0}{p_\varepsilon+p_0}\right),\\
&c_m = \frac{g}{M} - \gamma\left[\frac{K}{M}+f-1\right],\\
&\frac{k}{k_0} = \left(\frac{\varphi}{\varphi_0}\right)^3,
\end{aligned}\right\} \tag{5}$$

where φ is porosity; φ_0 is initial porosity; K is the bulk modulus in GPa; M is the constrained axial modulus in GPa; γ is the solid compressibility, which is also known as grain compressibility; p_s is atmospheric pressure under standard condition, which is expressed in MPa; and f is a fraction whose value varies between 0 and 1. A value of 0 and 1 is recommended for vertical and horizontal cleats, respectively.

In principle, the porosity-permeability or stress-permeability model is defined as the change in effective stress, which changes the internal structure of coal and rock fracture and deforms the matrix or even leads to its failure. The permeability of the rock mass is affected consequently. This is also the main theoretical principle for evaluating permeability enhancement and pressure relief of protective seam mining. Cheng et al. [25] proposed a theoretical model for permeability evolution and pressure relief of coal, which contains gas in deep PCSM. The existing ground stress in the

deep seam, which changes effective stress, was considered, and it controlled permeability directly or indirectly. Furthermore, the existing fractures as well as new fractures were further extended and governed by the PCSM process. The influence of coal matrix deformation on permeability alteration can be ignored. By assuming effective stress, gas adsorption/desorption, and strain as variables, a theoretical model for enhancing coal permeability was established [25]:

$$\frac{k}{k_0} = \left[1 + \frac{(\varepsilon_{V0} - \varepsilon_V) + f_m(\varepsilon_{m0} - \varepsilon_m)}{\varphi_0}\right]^3 \times \left[\frac{1-\varphi_0}{1-\varphi_0 - (\varepsilon_{V0} - \varepsilon_V) + f_m(\varepsilon_{m0} - \varepsilon_m)}\right]^2. \quad (6)$$

Here, ε is the strain, the subscript "0" refers to the initial point, the subscript "m" refers to the coal matrix, the subscript "V" refers to the volume, and f_m is the influence factor, which ranges between 0 and 1, and the desorption and shrinkage of the coal matrix affected the strain of fracture.

Because the relationship between permeability and stress is different for fractured and intact coal and rock masses, the failure of the rock mass between protective and protected seams was considered in any study, which was associated with GSM during PCSM.

3. Gas Seepage Model of Upper Protective Seam Mining

The gas seepage model (GSM) was established with upper PCSM, which mainly depends on the gas source and seepage media. The gas source is mostly dependent on the protected seam, and seepage media is largely associated with interbedded rock mass. As shown in Figure 1, King [26] determined various types of coal seam gas migration by using numerical simulation. In the protective seam mining process, a large amount of gas was desorbed from the bottom of the protective seam, providing pressure relief as well as coal and rock expansion. This was the main source of gas, which flows into PSWF through the interbedded rock mass.

Different failure mechanisms are associated with the interbedded rock mass, which depends on its lithology and its distance to the floor of the protective seam. The corresponding gas permeability also varies in this experiment. There are two types of interbedded rock masses, namely, elastic intact and plastic fractured rock masses. Flow process could be divided into three stages from the protected seam to PSWF: (1) gas desorption occurs by providing pressure relief in the protected seam, (2) the gas seepage stage occurs through the intact rock mass, and 3) the gas seepage stage occurs through the fractured rock mass. To simplify the developed model, the following assumptions were made for analysis:

(1) The entire model system has the same constant temperature

(2) The interaction between water and other gases was ignored, i.e., only gas is modeled

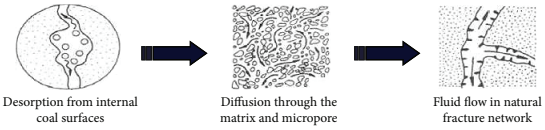

Figure 1: Gas transport mechanisms in the reservoir [26].

(3) Gas flows along the shortest path in the fractured rock

(4) Gas is regarded as an ideal gas; the dynamic viscosity and the diffusion coefficient are considered as constant values

Several studies show that there are three main states for in situ coal seam gas, namely, absorbed gas, free gas, and dissolved gas. In the process of pressure relief and expansion of the coal seam, the released gas was mainly absorbed with the formation of the coal seam. The desorption process works as the reverse mechanism of the absorption process, which is governed by the Langmuir equation [27]. In gas desorption stage, gas diffuses into elastic rock as pores of the intact rock mass are relatively small. The process of diffusion obeys an unsteady and nonequilibrium desorption model, which is known as Fick's second law.

$$Q = D \times \frac{c - c_0}{H} \times A. \quad (7)$$

Herein, Q is the quantity of gas diffusing in unit time, which is expressed in m^3/s; D is the diffusion coefficient; $c - c_0$ is the concentration difference; H is the distance of the cleat, which is expressed in meters; and A is the pore area, which is expressed in m^2. The normal gas is assumed to obey the state equation of ideal gas:

$$PV = NRT. \quad (8)$$

Herein, P is the ideal gas pressure, which is expressed in MPa; V is the ideal gas volume, which is expressed in m^3; N is the amount of substance of gas, which is expressed in mol; T is thermodynamic temperature of ideal gas, which is expressed in Kelvin; R is the ideal gas constant.

Equation 9 illustrates the relationship between the concentration of gas and the amount of gas substrate:

$$c = \frac{N}{V}. \quad (9)$$

Gas pressure of the protective seam was denoted as P_1, and the distance was denoted as H. Gas pressure of intact rock mass was assumed to be equal to atmospheric pressure (P_0). Equation (10) was used for calculating gas quantity (Q_1), which diffuses into intact rock mass:

$$Q_1 = D \times \frac{p_1 - p_0}{HRT} \times A. \quad (10)$$

When gas diffuses into the intact rock mass, it enters the seepage stage of intact and fractured rock masses.

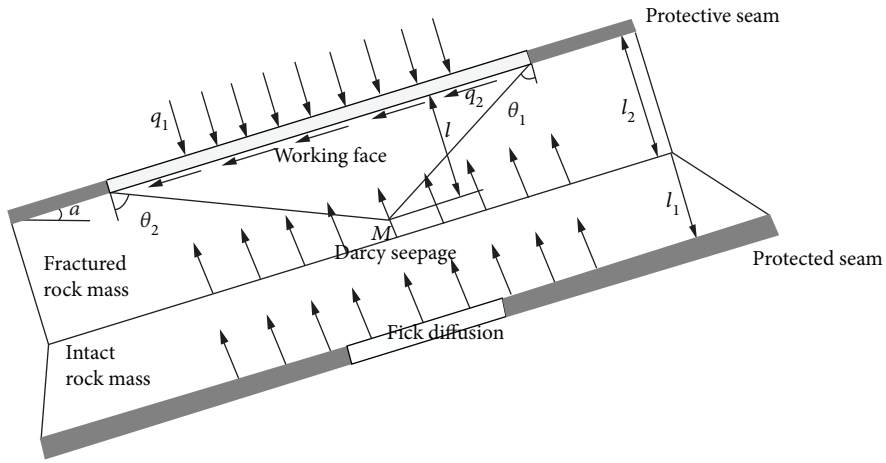

Figure 2: Coal seam gas diffusion and seepage.

Equation (11) shows that gas seepage in the rock mass follows Darcy's Law.

$$Q = K \times \frac{P - P_0}{\mu l} \times A. \tag{11}$$

Here, Q is the quantity of seepage gas, which is expressed in m^3/s; K is permeability of rock, which is expressed in m^{2-}; $P - P_0$ is the pressure difference, which is expressed in Pa; l is the distance of seepage, which is expressed in meters; A is seepage area, which is expressed in m^2; and μ is the dynamic viscosity coefficient, which is expressed in MPa·s. Equation (12) was used to calculate gas pressure after the stage of intact rock mass. As shown in (12), the vertical length of the intact rock mass is known as l_1. According to flow conservation principle, the permeability of the intact rock mass is known as k_2.

$$p_z = p_1 - \frac{D\mu l_1 (p_1 - p_0)}{k_2 HRT}. \tag{12}$$

Gas flows (Q_2) from the protected seam to PSWF in fractured rock mass, which was calculated by utilizing (13). Rock permeability is called k_3, l_2 is called vertical length, and ventilation pressure of PSWF is p_2.

$$Q_2 = \left[\frac{p_1 - p_2}{\mu l_2} - \frac{D\mu l_1 (p_1 - p_0)}{k_2 HRT}\right] k_3 A. \tag{13}$$

After PCSM, (14) was used for calculating maximum and minimum principle stresses at any point for the fractured rock mass [28].

$$\sigma_1, \sigma_3 = \frac{q_1}{\pi}\theta \pm \frac{1}{\pi}\left(\sqrt{{q_1}^2 + {q_2}^2}\sin\theta + q_2\theta\right) + \frac{\gamma l}{\cos\alpha}. \tag{14}$$

Herein, q_1 is the vertical stress that acts on the floor, which is expressed in MPa; q_2 is the horizontal stress, which is expressed in MPa; and α is the angle of the coal seam, which is expressed in degrees. As shown in Figure 2, $\theta = \theta_1 - \theta_2$, where θ_1 and θ_2 are angles of the connection between the point and the floor, and they are also expressed in degrees; l is the vertical distance between the point M and the floor of the protective seam, which is expressed in meters; and γ is the rock density, which is expressed in MN/m^3.

The permeability-stress model was chosen for determining permeability of intact and fractured rock masses. By using laboratory data fitted with (3) and (4), the shortest path was chosen, i.e., $\theta = 0$. Suppose that stress of the intact rock mass is γl, the original rock mass stress is γh, and h is the buried depth of the protected seam. This assumption is based on the fact that in the actual production process, most gases released from the protected seam do not diffuse into PSWF. By continuously advancing the working face, gas pressure of the protected seam is reduced gradually. Equation (15) must be multiplied with a loss of coefficient δ. By substituting parameters into (13), (15) is obtained as follows:

$$\begin{aligned} Q_2 &= \frac{A\delta\left(p_1 - (D\mu l_1 (p_1 - p_0))/\left(k_0 HRT\int_0^{l_1} e^{-0.25\gamma(l_1+l_2-h-x)}dx\right) - p_2\right)\int_0^{l_2} k_1 (\gamma x/\cos\alpha)^m dx}{\mu l_2} \\ &= \frac{\left(p_1 - (D\gamma\mu l_1 (p_1 - p_0))/\left(4k_0 HRT\left[e^{-0.25\gamma(l_2-h)} - e^{-0.25\gamma(l_1+l_2-h)}\right]\right) - p_2\right) A\delta k_1 \gamma^m {l_2}^m}{(m+1)\mu\cos^m\alpha}. \end{aligned} \tag{15}$$

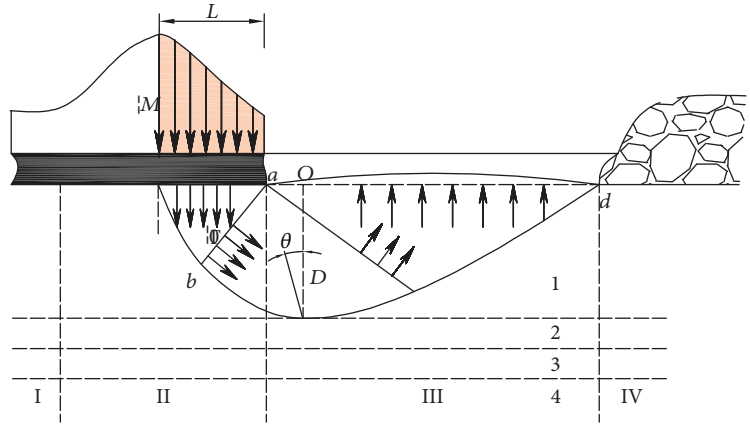

Figure 3: Floor failure depth caused by the bearing pressure.

Figure 2 summarizes the entire GSM of the upper PCSM.

Equation (15) shows that there are three main factors associated with gas quantity, which can cause gas to flow into PSWF from the protected seam, namely

(1) the initial gas pressure of the protected seam

(2) interlayer spacing of interbedded rock mass, the percentage of fractured and intact rock mass, and the permeability coefficient of fractured and intact rock mass

(3) the ventilation pressure of PSWF and seepage area of the floor

4. Analysis of Floor Failure Depth

4.1. Theoretical Calculation Model for Floor Fracture Development Depth. The most significant part of the analysis is to determine floor failure depth according to GSM of the protected seam, which was introduced in Section 3. The methods of calculating floor failure depth consisted of theoretical calculation and empirical regression equation.

The coal mining process transfers the overburden load to the coal body ahead of the working face and compacts falling rock in the goaf by forming a peak region for bearing pressure. In front of the working face, the floor rock was in a state of compression, experiencing compressive displacement. In the goaf behind the working face, the floor rock was in a stress relief zone, and it experienced expansive displacement. Shear failure normally occurs in floor rocks because of shear deformation, which are located at the border of compression and expansion regions. In a conventional advancing process of the working face, there are three stages of stress in the floor: stress escalation before mining, stress drop after mining, and stress recovery. These stages of stress repeatedly occur with advancing of the working face. In surrounding floor areas of the working face, stress distribution on the floor rock mass was affected by mining. It was divided into four horizontal regions: (1) original rock stress region, (2) compression region, (3) expansion region, and (4) stress recovery region. The distribution of floor strata was divided into the following four vertical zones: (i) broken zone, (ii) newly damaged zone, (iii) originally damaged zone, and (iv) fractured zone [29]. Figure 3 shows the areas of the floor, which were influenced by bearing pressure.

According to elastic-plastic mechanics and Mohr-Coulomb strength theory, a plastic zone was formed in the floor rock with plastic deformation. It was within a certain range of the working face floor when bearing pressure reached or exceeded the pressure limit value.

When the bearing pressure reached maximum capacity, part of the rock failed completely by joining plastic zones of rock mass in the surrounding region of bearing pressure. With plastic deformation of the rock mass, a continuous slip surface is formed in the goaf direction.

The maximum failure depth of the floor, which is caused by stress concentration under ultimate bearing pressure conditions of the floor rock, can be obtained by using (16). The ultimate bearing capacity of strata was calculated using Mohr-Coulomb failure criterion [30].

The width of the plastic area was calculated by using (16). Equation (17) was used for determining the maximum failure depth of the floor.

$$L' = a \times \left(\frac{1}{\sqrt{1 - \left(n_m \gamma H / (2\sigma_M + n_m \gamma H)\right)^2}} - 1 \right) \tag{16}$$

or $L' = 0.015H$,

$$h = \frac{L' \cos \beta}{2 \cos\left(\pi/4 + \beta/2\right)} \times e^{(\pi/4+\beta/2)\times \tan \beta}. \tag{17}$$

Here, a, which is expressed in meters, is twice of roof-control distance in the working face; n_m is the maximum coefficient of stress concentration; σ_M is the ultimate stress of the coal body edge, which is expressed in MPa; H is the vertical distance from the working face to the ground surface, which is expressed in meters; and β is the internal friction angle of floor strata, which is expressed in degrees.

Table 1: Physical and mechanical parameters of the rock and coal.

Serial number	Lithology	Thickness (m)	Density (kg·m^{-3})	Bulk modulus (GPa)	Shear modulus (GPa)	Cohesion (MPa)	Internal friction angle (°)	Strength of extension (MPa)
1	Fine sandstone	8.01	2500	3.0	1.5	2.0	35	1.5
2	Siltstone	2.99	2400	2.6	1.6	2.2	36	1.5
3	Coal line	0.49	1450	1.8	1.0	1.5	30	1.0
4	Siltstone	3.67	2500	2.6	1.6	2.2	36	1.5
5	Fine sandstone	4.23	2500	2.9	1.9	2.8	39	1.8
6	2# coal seam	1.00	1450	1.8	1.0	1.5	30	1.0
7	Sandy mudstone	2.58	2300	2.0	1.3	2.0	38	1.5
8	Siltstone	4.92	2400	2.6	1.6	2.2	36	1.5
9	Middle-fine sandstone	8.11	2600	4.0	2.4	2.8	38	2.8
10	Siltstone	1.98	2400	2.6	1.6	2.2	36	1.5
11	3# coal seam	6.09	1400	1.8	1	1.5	30	1.0
12	Sandy mudstone	2.97	2400	2.0	1.3	1.5	30	1.2
13	Fine sandstone	5.03	2500	2.8	1.8	2.9	36	1.7
14	Middle-fine sandstone	45.64	2500	3.0	1.5	2.0	35	1.5

Equation (18) is used for theoretical calculation of failure depth of the floor [31].

$$h = \frac{1.57\gamma^2 H^2 L}{4{R_c}^2}. \tag{18}$$

Here, h is the depth of the broken zone and L is the length of the working face, both of which are expressed in meters, and R_c is the uniaxial compressive strength of the rock, which is expressed in MPa.

In previous studies, statistical analysis was conducted to determine failure depth of the floor during the coal mining process in various mines. Corresponding linear regression equation was formed by using multivariate linear and nonlinear statistical analysis methods. Some of the typical equations are as follows [31–33]:

$$h = 0.0113H + 6.25 \ln\left(\frac{L}{40}\right) + 2.52 \ln\left(\frac{M_h}{1.48}\right), \tag{19}$$

$$h = 0.0111L + 0.006H + 4.541f_c - 0.009\alpha - 2.4, \tag{20}$$

$$h = -2.0234 + 1.48 \times 10^{-26} H^9 + 0.1016L + 0.1913\alpha + 1.0637M_h - 5.5536D + 7.5070I. \tag{21}$$

Here, M_h is the mining height of the coal seam, which is expressed in meters; D is the failure resistance capability of the floor; and I is the factor related to existence of cutting fault or failure situation of the broken zone. By utilizing the aforementioned equations for estimating floor failure depth, the length of intact and fractured rock masses in GSM was obtained.

For a case study in a certain coal mine in Hancheng city, Shanxi province, China, the verification procedure and associated calculations are described in the following subsections.

The actual two PSWFs were used to verify the model. The distance along the strike was 1142 m, with 180 m of inclined width for PSWF4216. For PSWF4215, the distance along the strike is 1158 m with 200 m of inclined width. These two working faces are located in the No.2 coal seam; the thickness of the coal seam was about 0–2.5 m and the average thickness was 1 m. The depth of the No.2 coal seam was 430 m. The spacing of the No.2 coal seam and the underlying No.3 coal seam (the protected seam) was in the range of 9.8–20.7 m, with the average spacing being 15.5 m. The gas content of this protective coal seam is not high, and the pressure was 0.55 MPa. The lower No.3 coal seam had outburst risk. When the relative gas emission of the No.3 coal seam rose to 27.82 m^3/t, gas pressure became 2.03 MPa and coal seam was of low permeability. Table 1 shows the surrounding rock of the working face and mechanical parameters of the rock mass. Figure 4 shows the borehole diagram of the working face.

In order to verify the accuracy of the developed GSM in the protected seam, floor failure depth during excavation process of the working face was determined first. Using theoretical equations (16)–(18) and the data obtained from mining (H is 430 m, β is 40°, L is 180 m, γ is 0.025 kg/cm^3, and R_c is 21.59 MPa), the failure floor depths were estimated to be 15.2 m and 17.52 m. Using regression equations 19–21 and the obtained values (M_h is 1.2 m, α is 0°, D is 0.2, I is 0, and f is 3), floor failure depths were estimated to be 13.73 m, 15.80 m, and 16.44 m. By considering the results of both theoretical and regression equations, the calculated floor failure depth was found to be in the range of 13.73 to 17.52 m, with an average failure depth of 15.625 m. This value was found to be very close to the actual average interlayer spacing in the mine. To further determine failure depth of the floor,

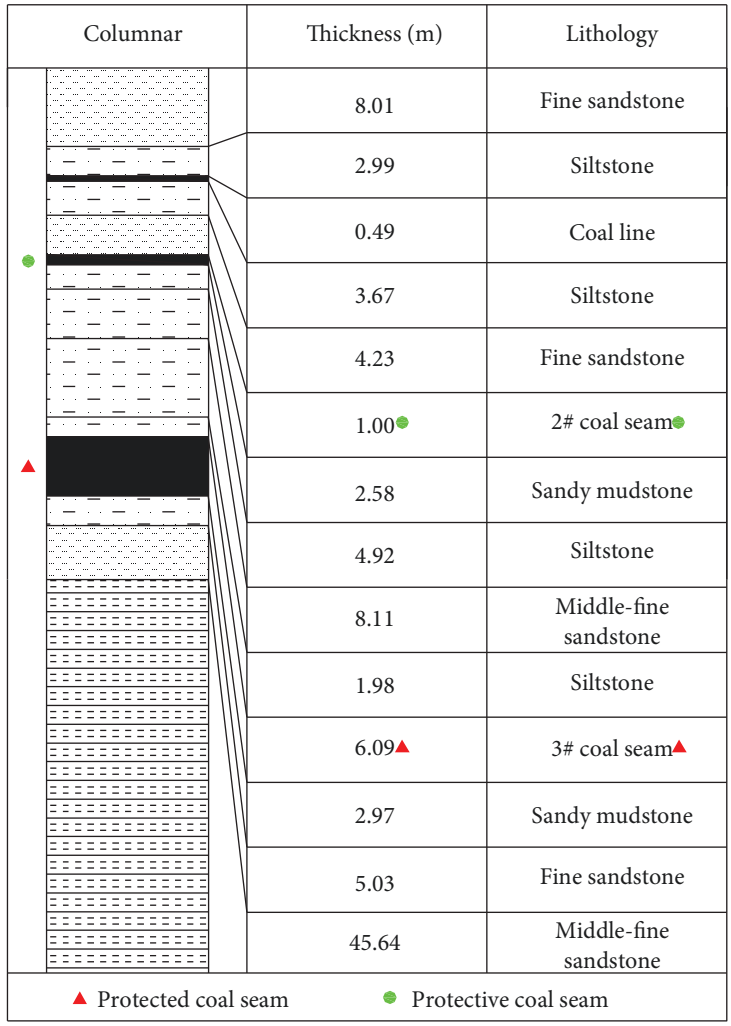

Figure 4: Borehole diagram of the working face.

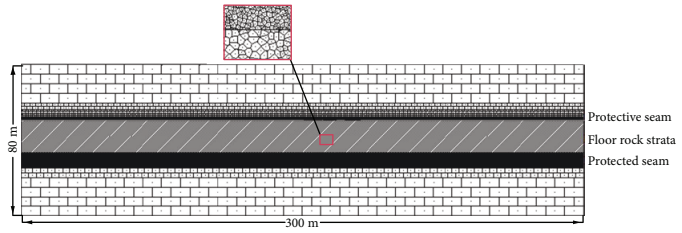

Figure 5: Schematic diagram of the numerical model.

numerical analysis was carried out by using UDEC numerical simulation software.

4.2. Numerical Simulation for Floor Fracture Development Depth. The Mohr-Coulomb constitutive model was used for simulation, and rock mechanics parameters are presented in Table 1. A schematic diagram of the model is presented in Figure 5. The length of the model was 300 m, and it has a width of 80 m. The roof of the protective seam was divided into a layered structure by using JSET. Structural breakage was not observed in the floor strata between the protective and protected seams, which were similar to the roof of the protective seam. Strata and rock parameters had different thicknesses. As shown in Figure 5, floor strata were divided into a polygon with congruent sides by using the 2D VORONOI polygon generator. In this numerical model, deformable and rigid polygons are available in UDEC. However, individual polygons cannot break, i.e., all fractures must follow polygonal boundaries. The cemented contacts between two polygons can rupture through shear or tension depending on the stress state and properties of the contact surface. Therefore, fracture development can be realistically simulated through the contact rupture initiation, growth, and nucleation. The force-displacement relationship for a contact

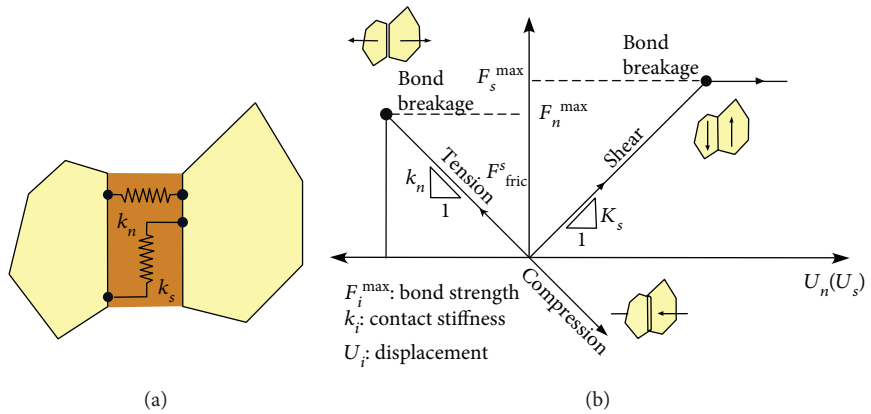

Figure 6: Constitutive model of the contact in UDEC: (a) normal and shear stiffness between blocks; (b) constitutive behavior in shear and tension (i = s, n) [34].

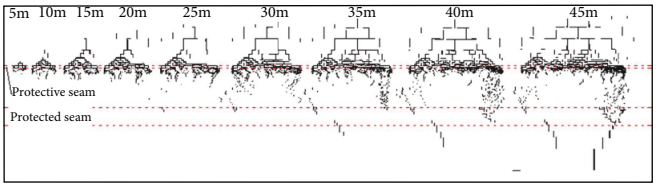

Figure 7: Floor fracture depth diagram with the different advancing distance.

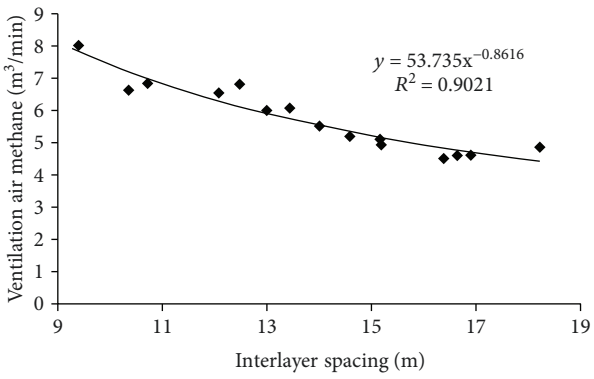

Figure 8: Scatter diagram of the ventilation air methane for PSWF4216.

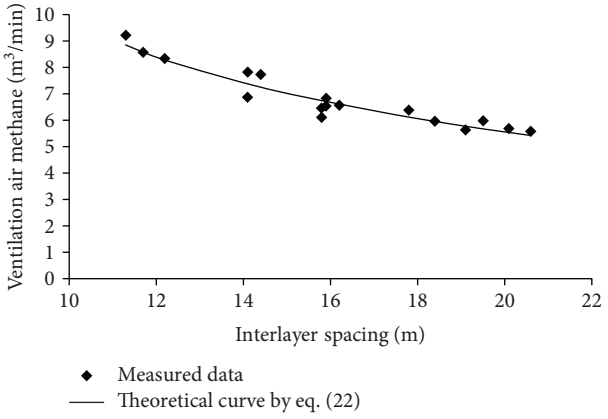

Figure 9: The measured data and the theoretical curve of PSWF4215.

is determined by normal (K_n) and shear (K_s) stiffness of the contact. The contact properties, cohesion, tensile strength, and friction angle define the contact strength. Fractures are created when the stress level at the interface exceeds a threshold value in either the tension or shear. The constitutive contact model is shown in Figure 6.

The PSWF starts excavation 50 m away from the left side edge of the model, excavating 5 m at each step for a 100 m distance. Figure 7 illustrates that the working face of advancing floor fractures develops gradually in depth while the range of fracture development enlarges continuously. When PSWF achieves an advancing distance of 30 m, the rock mass between protective and protected seams is connected by fractures but the development of fracture is sparse. The development gets more intensive when the advancing distance is 35 m. At an advancing distance of 40 m, the protected seam is covered by fractures. This causes the gas to desorb from the protected seam and flow into PSWF.

Based on the results of the numerical simulation and theoretical calculations, it was inferred that floor fracture develops on the protected seam during the PCSM process. Consequently, it can be considered that there is no intact rock mass between protective and protected seams. This assumption was deliberated in the following calculations.

5. Gas Seepage Model Verification

It is challenging to physically measure most of the parameters in GSM, while some parameters remain unchanged under same geological conditions. However, it can be concluded

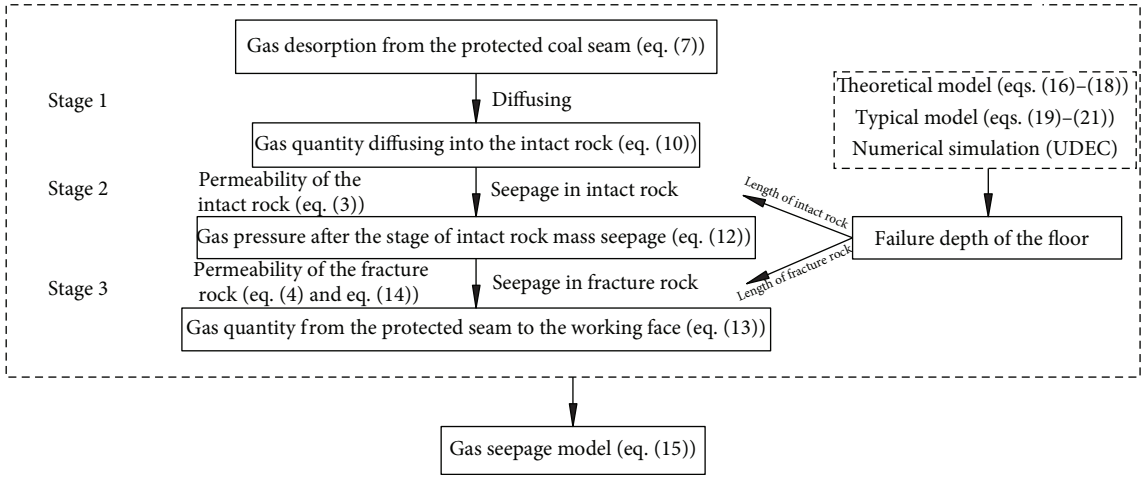

Figure 10: Calculation process of the gas seepage model.

from the aforementioned analysis that interbedded rock masses are all fractured rock masses. Equation (15) can be simplified into

$$Q_2 = \frac{(p_1 - p_2)A\delta k_1(\gamma l_2)^m}{(m+1)\mu}. \tag{22}$$

Based on the actual data for the considered PSWF4216 in Hancheng, China, the parameters associated with gas are as follows: $P_1 = 2.03$ MPa (the gas pressure of the protected coal seam), $P_2 = 0.1$ MPa (the gas pressure of PSWF), $\gamma = 0.025$ MN/m^3, and the floor area (inclined width of PSWF × floor width) of the working face is 180 m^2 and 200 m^2 for PSWF4216 and PSWF4215, respectively. The value of μ for gas is 1.75×10^{-11} MPa·s. The m and k_1 are assigned as -0.8616 and 2.613×10^{-13} m^2, respectively, which were introduced in the literature [22]. By substituting the above data into (22), the gas emission from the protected face was calculated by using

$$Q_g\left(\mathrm{m}^3/\mathrm{min}\right) = 60Q_2 = 53986.01 \times \delta l^{-0.8616}. \tag{23}$$

Between protective and protected seams, the altering values associated with interlayer spacing were obtained from a gas drainage borehole. This was placed in the floor of the air return gateway. After the working face advances to a distance of 30 m, floor fractures of PSWF can develop into the protected seam. The data from ventilation air methane in the working face were also used after it advances to a distance of 30 m. As shown in Figure 8, the scatter diagram and fitting curve of ventilation air methane were obtained with interlayer spacing of PSWF4216 along the corresponding interlayer spacing data.

The loss coefficient (δ) was calculated by using the scatter diagram of ventilation air methane (Figure 8). The correlation coefficient (R^2) of the fitting equation was 0.9022, which shows an acceptable fitting situation for engineering measured data. These findings confirm that (22) was used for calculating gas emission quantity in the protective seam, which corresponds precisely with field measurement. In addition, a loss coefficient (δ) of 1.012×10^{-3} was obtained. In order to further verify the correctness of GSM, the loss coefficient (δ) of 1.012×10^{-3} and parameters of PSWF4215 (only the floor area of PSWF4215 was different from PSWF4216.) were substituted into (22). Figure 9 shows the theoretical curve, which was drawn according to (22) of PSWF4215. Figure 9 shows that the measured data can match well with the theoretical curve, which further validates the feasibility and effectiveness of the proposed GSM.

6. Discussions

In the process of deep seam mining, PCSM has become one of the most significant measures of regional outburst mitigation as the inherent outburst risk is high. During the PCSM process, the phenomenon of methane concentration exceeding the limit usually occurs in the working face. It is very important to understand the factors affecting gas emission of PSWF and to develop an equation for calculating its quantity. In this study, a GSM was developed for the process of the upper PCSM. Using the equation of GSM, the quantity of gas desorbed from the protected seam into the protective seam was estimated. Fick's second law of diffusion and Darcy's flow law were used for this estimation. Moreover, the relationship between permeability and stress was investigated in an elastic-plastic state. The mechanics of the surrounding rock was also investigated in this paper. There are four assumptions and several simplifications used in the establishment of GSM; it greatly simplifies computational complexity and reduces the selection of parameters in engineering calculations. As shown in (15), it is simpler and easier to use GSM. This model does not need to spend a lot of time and money for additional field tests, and there are no additional uncertainty factors in GSM. For engineering application, this model has distinctive advantages and high efficiency. However, temperature, gas component, and moisture content are factors governing assumptions and simplifications. They also affect the permeability of coal and rock, reducing the

accuracy of the model. In future work, the above factors are considered in GSM.

7. Conclusions

In the process of PCSM, surrounding rock permeability was divided into two types, namely, failure plastic and elastic rock masses. The relationships between rock permeability and stress were also summarized under these two evolution types, which provides theoretical basis for GSM between protective and protected seams. Eventually, gas emission from the protected seam was classified in three stages, namely, (1) the gas desorption stage from the protected seam with pressure relief, (2) the gas seepage stage in the intact rock mass, and (3) the gas seepage stage in fractured rock mass (Figure 10). From these equations, it can be concluded that the initial gas pressure of the protected seam, the characteristics of interlayer rocks, and the ventilation pressure of the working face were the main influencing factors of gas emission quantity, which flowed from the protected coal seam to PSWF.

The actual geological conditions of a protective seam were investigated in a coal mine, which was located in Hancheng, China. The GSM was used to calculate gas emission quantity from the protected seam. The modeling results correspond precisely with field measurement by considering the fitting curve of ventilation air methane quantity for PSWF4216 and PSWF4215 with an interlayer spacing and loss coefficient (δ) of 1.012×10^{-3}. It is worth noting that actual conditions are simplified by the model proposed in this paper. These conditions were based on some aforementioned assumptions. In future study, gas emission from the goaf and its influencing factors were identified. Furthermore, some of the parameters in these equations were adjusted based on the analysis of additional field data measurements from the working face of the PCSM process. Future study will help us to further mitigate gas accumulation risk in the PCSM process.

Data Availability

The data used to support the findings of this study are available from the corresponding author upon request.

Conflicts of Interest

The authors declare that they have no conflicts of interest.

Acknowledgments

Financial support for this work was supported by the Beijing Natural Science Foundation (8184082); the National Natural Science Foundation of China (Nos. 51704274, 51502339, and 51704278); the First-Class Professional Construction of Undergraduate Colleges in Guizhou Province (SJZY2017006); the Open Projects of State Key Laboratory of Coal Resources and Safe Mining, CUMT (SKLCRSM16KF 06); Young Scientists and Technicians Growth Project of Guizhou Education Department (Qian Ke He KY Zi[2018]115); and the Yue Qi Distinguished Scholar Project, China University of Mining & Technology, Beijing.

References

[1] Y. W. Liu and G. F. Li, "Reliability research of protective layer mining and pressure-relief gas drainage," *Journal of Mining & Safety Engineering*, vol. 3, pp. 426–431, 2013.

[2] A. Liu, S. Tu, F. Wang, Y. Yuan, C. Zhang, and Y. Zhang, "Numerical simulation of pressure relief rule of upper and lower protected coal-seam in thin-protective-seam mining," *Disaster Advances*, vol. 6, pp. 16–25, 2013.

[3] J. H. Fu and Y. P. Cheng, "Situation of coal and gas outburst in China and control counter measures," *Journal of Mining & Safety Engineering*, vol. 24, no. 3, pp. 253–259, 2007.

[4] W. A. Chao, S. O. Da-zhao, and D. U. Xue-sheng, "Prediction of coal and gas outburst based on distance discriminant analysis method and its application," *Journal of Mining & Safety Engineering*, vol. 4, pp. 470–447, 2009.

[5] J. Han, H. W. Zhang, W. H. Song, and Z. Wang, "In-situ stress field of coal and gas outburst mining area," *Chinese Journal of Rock Mechanics and Engineering*, vol. 2, pp. 3852–3859, 2008.

[6] C. Zhang, S. Tu, L. Zhang, and M. Chen, "A study on effect of seepage direction on permeability stress test," *Arabian Journal for Science and Engineering*, vol. 41, no. 11, pp. 4583–4596, 2016.

[7] C. Zhang, S. Tu, Q. Bai, G. Yang, and L. Zhang, "Evaluating pressure-relief mining performances based on surface gas venthole extraction data in longwall coal mines," *Journal of Natural Gas Science and Engineering*, vol. 24, pp. 431–440, 2015.

[8] C. Zhang, S. Tu, L. Zhang, Q. Bai, Y. Yuan, and F. Wang, "A methodology for determining the evolution law of gob permeability and its distributions in longwall coal mines," *Journal of Geophysics and Engineering*, vol. 13, no. 2, pp. 181–193, 2016.

[9] F. Wang, T. Ren, S. Tu, F. Hungerford, and N. Aziz, "Implementation of underground longhole directional drilling technology for greenhouse gas mitigation in Chinese coal mines," *International Journal of Greenhouse Gas Control*, vol. 11, no. 6, pp. 290–303, 2012.

[10] C. Ö. Karacan, F. A. Ruiz, M. Cotè, and S. Phipps, "Coal mine methane: a review of capture and utilization practices with benefits to mining safety and to greenhouse gas reduction," *International Journal of Coal Geology*, vol. 86, no. 2-3, pp. 121–156, 2011.

[11] C. Zhang, S. Tu, M. Chen, and L. Zhang, "Pressure-relief and methane production performance of pressure relief gas extraction technology in the longwall mining," *Journal of Geophysics and Engineering*, vol. 14, no. 1, pp. 77–89, 2016.

[12] Y. Lv, "Test studies of gas flow in rock and coal surrounding a mined coal seam," *International Journal of Mining Science and Technology*, vol. 22, no. 4, pp. 499–502, 2012.

[13] Y. Q. Tao, J. Xu, S. C. Li, X. J. Tang, and M. J. Cheng, "Integrated control technology for methane in mining faces," *Journal of Chongqing University*, vol. 9, pp. 1068–1073, 2008.

[14] L. Zhang, T. Ren, and N. Aziz, "Influences of temperature and moisture on coal sorption characteristics of a bituminous coal from the Sydney Basin, Australia," *International Journal of Oil, Gas and Coal Technology*, vol. 8, no. 1, pp. 62–78, 2014.

[15] L. Zhang, T. Ren, N. Aziz, and S. Tu, "Triaxial permeability testing and microstructure study of hard-to-drain coal from Sydney Basin, Australia," *International Journal of Oil, Gas and Coal Technology*, vol. 8, no. 4, pp. 432–448, 2014.

[16] W. Yang, B. Q. Lin, Q. Yan, and C. Zhai, "Stress redistribution of longwall mining stope and gas control of multi-layer coal seams," *International Journal of Rock Mechanics and Mining Sciences*, vol. 72, pp. 8–15, 2014.

[17] V. Palchik, "Use of Gaussian distribution for estimation of gob gas drainage well productivity," *Mathematical Geology*, vol. 34, no. 6, pp. 743–765, 2002.

[18] I. Palmer, "Permeability changes in coal: analytical modeling," *International Journal of Coal Geology*, vol. 77, no. 1-2, pp. 119–126, 2009.

[19] I. Gray, "Reservoir engineering in coal seams: part 1-the physical process of gas storage and movement in coal seams," *SPE Reservoir Engineering*, vol. 2, no. 1, pp. 28–34, 1987.

[20] J. P. Seidle, D. J. Jeansonne, and D. J. Erickson, "Application of matchstick geometry to stress dependent permeability in coals," in *Proceedings of SPE Rocky Mountain Regional Meeting*, pp. 433–444, Wyoming, May 1992.

[21] T. X. Ren and J. S. Edwards, *Goaf Gas Modelling Techniques to Maximize Methane Capture from Surface Gob Wells*, S. E. De, Ed., Mine Ventilation, 2002.

[22] D. N. Whittles, I. S. Lowndes, S. W. Kingman, C. Yates, and S. Jobling, "Influence of geotechnical factors on gas flow experienced in a UK longwall coal mine panel," *International Journal of Rock Mechanics and Mining Sciences*, vol. 43, no. 3, pp. 369–387, 2006.

[23] I. Palmer and J. Mansoori, "How permeability depends on stress and pore pressure in coalbeds: a new model," *SPE Reservoir Evaluation & Engineering*, vol. 1, no. 6, pp. 539–544, 1998.

[24] I. Palmer, M. Mavor, and B. Gunter, "Permeability changes in coal seams during production and injection," in *International Coalbed Methane Symposium, University of Alabama*, Tuscaloosa, Alabama, 2007.

[25] Y. P. Cheng, H. Y. Liu, P. K. Guo, R. K. Pan, and L. Wang, "A theoretical model and evolution characteristic of mining-enhanced permeability in deeper gassy coal seam," *Journal of China Coal Society*, vol. 39, no. 8, pp. 1650–1658, 2014.

[26] G. R. King, *Numerical Simulation of the Simultaneous Flow of Methane and Water through Dual Porosity Coal Seams during the Degasification Process, [Ph.D. Dissertation]*, Pennsylvania State University, 1985.

[27] J. Shi, X. Li, B. Xu et al., "Review on desorption-diffusion-flow model of coal-bed methane," *Scientia Sinica Physica, Mechanica & Astronomica*, vol. 43, no. 12, pp. 1548–1557, 2013.

[28] J. Sun, "Failure characteristics of floor "three-zone" along the inclined direction of coal seam," *Journal of Mining & Safety Engineering*, vol. 1, pp. 115–121, 2014.

[29] L. Q. Shi and J. Han, "Theory and practice of dividing coal mining area floor into four-zone," *Journal of China University of Mining & Technology*, vol. 34, no. 1, pp. 16–23, 2005.

[30] M. G. Qian and P. W. Shi, *Mine Pressure and Strata Control*, China University of Mining and Technology press, Xuzhou, 2003.

[31] L. Q. Shi, D. J. Xu, M. Qiu, X. Jing, and H. H. Sun, "Improved on the formula about the depth of damaged floor in working area," *Journal of China Coal Society*, vol. 38, no. 2, pp. 299–303, 2014.

[32] Y. B. Guan, H. M. Li, and J. C. Lu, "Research of no. 9 coal seam floor's fracture regularity in Xian Dewang coal mine," *Journal of China Coal Society*, vol. 28, no. 2, pp. 121–125, 2003.

[33] Y. Zhang, "The induced function of mining pressure to the damage of the floor," *Journal of Taiyuan University of Technology*, vol. 33, no. 3, pp. 252–256, 2002.

[34] A. Lisjak and G. Grasselli, "A review of discrete modeling techniques for fracturing processes in discontinuous rock masses," *Journal of Rock Mechanics and Geotechnical Engineering*, vol. 6, no. 4, pp. 301–314, 2014.